Banana Plant Waste Rotary Dryer Design and Simulation Using 3D Computer Aided Design

Ray H. Malonjao [1], Juvy B. Malonjao [2], Ronald M. Galindo [3]

[1] *Faculty, Mechanical and Aerospace Engineering, Cebu Technological University-Main Campus,*
M.J. Cuenco Ave., Corner R. Palma St., Cebu City, 6000, Cebu, Philippines
[2] *Faculty, Industrial Engineering, Cebu Technological University-Main Campus,*
M.J. Cuenco Ave., Corner R. Palma St., Cebu City, 6000, Cebu, Philippines
[3] *College of Engineering, Cebu Technological University-Main Campus,*
M.J. Cuenco Ave., Corner R. Palma St., Cebu City, 6000, Cebu, Philippines

Abstract – **This research determines the optimal rotary dryer design for banana waste drying with Biot number. When banana waste is adequately dried, it can be repurposed into valuable resources. Based on the proposed banana plant waste rotary dryer, drying efficiency is significantly improved compared to conventional dryers as attributed to design calculations and simulation. Here, the design process involves the three-dimensional (3D) computer-aided design of individual parts, subassemblies, and main assembly, accompanied by detailed illustration drawings, and optimization of rotary dryer flight design. Biot number is crucial in the design calculations of the diameter and length of the dryer. The Design of Experiments (DoE) and computational fluid dynamics simulations are also used. Proper drying, facilitated by the proposed rotary dryer, enables efficient repurposing of banana waste into animal feed, biofuel, bioplastics, and other nanotechnology applications, contributing to sustainable waste management practices and a promising solution to environmental challenges.**

1. Introduction

Global demand for fruits, notably bananas, had risen due to population growth and dietary shifts, with the world banana trade reaching an unprecedented 21 million tons in 2019 [1]. Bananas, recognized for their appealing taste and texture, were noted to be rich in dietary fiber, vitamins, and minerals, offering nutritional benefits and aiding digestion [3]. Phenolic compounds in bananas were found to have functional properties, inhibiting lipid oxidation and microbial growth, potentially contributing to health benefits such as reduced cancer and heart disease risk [4]. In 2020, global fruit production was projected to reach a million metric tons, with bananas contributing significantly [2].

Recovering secondary metabolites from bananas yielded valuable ingredients, enhancing profitability in the banana industry [4], [5], [6]. The United Nations Food and Agriculture Organization reported a significant increase in banana output globally, notably in Ecuador and the Philippines, with an anticipated market expansion of 135 million tons by 2028 [6]. In 2019, banana exports reached 20.2 million tons, led by India (30.4 million tons) and China (11.6 million tons) [1], [7]. Despite this growth, the food industry, a major waste producer, contributed about 70% of global agricultural waste [8]. Efficient utilization of banana by-products was thought of as a means that could mitigate waste and further benefit the industry.

Despite the abundance of banana plant waste, its utilization was limited due to factors like high fiber content in stems and leaves.

Banana waste comprised small, mangled, or rotten fruits, peels, stalks, and pseudo-stems, with fruits constituting 25.2% and pseudo-stems/leaves making up 74.8% of aboveground plant components [9]. Typically considered low value, these by-products were often composted, landfilled, or discharged into waterways, posing environmental harm. Due to high moisture content and susceptibility to spoilage, these by-products were frequently wasted [10]. Examples included shoots, flowers, crowns, leaves, and discarded fruits, potentially contributing to environmental issues based on biodegradability and volume generated.

A number of sources mentioned that approximately a third of banana for production was rejected for not meeting quality criteria, potentially serving as valuable waste-to-value products, resulting in more than three quarters of the entire plant being considered waste. The United Nations' Food and Agriculture Organization categorized waste into losses and waste, with agricultural production and processing contributing to losses [11].

In the Philippines, the Ecological Solid Waste Management Act (R.A. No. 9003) addressed the waste issue resulting from population growth, but challenges include non-segregation of waste, inconsistent collection, insufficient vehicles, inadequate recovery facilities, and limited government funding [12]. These obstacles hindered the effective execution of waste management efforts [12].

Extensive research explored the potential applications of various banana byproducts, such as peels, leaves, pseudo-stems, pseudo-stem juice, stalks, and inflorescence, across industries. These applications include their use as a thickening agent, an alternative source of nutraceuticals, renewable energy, coloring agents, natural fibers, biofertilizers, bioactive compounds, and livestock feed [9]. To enhance the utility of banana waste, additional processing was required to eliminate moisture and preserve the byproducts due to their high-water content. Processing banana waste into value-adding products proved to be a cost-effective alternative compared to disposal in landfills or mere mixing with soil [14]. A significant challenge in this process was the necessity for drying, which traditionally faces economic inefficiencies, particularly during the rainy or wet season.

Transforming banana waste into profitable waste-to-value products posed a challenge in efficiently processing such with an environmentally friendly drying mechanism, emphasizing the engineering, modeling, and optimization of rotary dryer-based drying for banana solid waste. Various dryers, particularly rotary dryers, had been extensively studied for their modeling and optimization to achieve effectiveness and economic efficiency [15]. Drying, a complex non-linear process involving particle movement and heat, posed challenges for conventional modeling and regulation of rotary dryers [15]. Factors influencing rotary dryer modeling included the physical characteristics of solids, dryer variables, and operational conditions. The study by Areed et al. contributed insights into the detailed dynamics of the drying process [15]. For a long time, the use of rotary dryers was regarded as the best and most effective drying method for solid particles because of its simplicity, adaptability, and enormous capacity. Rotary dryers had the highest construction costs but the lowest operational costs when compared to fluidized and conveyor belt dryers [16].

In a study by Kiranoudis et al. [17], rotary dryers were found to require significantly less supervision compared to fluid bed dryers and were less affected by changes in feedstock, even during reduced feed conditions. Mirade and Daudin [18] emphasized the importance of air in drying efficiency, stating that computational fluid dynamics (CFD) simulations could determine factors like temperature, fluid flow rate, and airflow direction and speed in the drying chamber. CFD simulation provided detailed information on mass and heat transfer, enabling the evaluation of adjustments to dryer geometric design using input parameter data. The study of Rindang et al. [19] confirmed, through experimental and CFD modeling, that three-dimensional (3D) computer aided design (CAD) CFD simulation accurately predicts temperature distribution in the dryer during the drying process.

2. Materials and Methods

The rotary dryer design and simulation model, as outlined in the study, provided a systematic approach for developing an efficient drying system. Beginning with project conceptualization, crucial parameters like material characteristics and desired moisture content were identified. A literature review and preliminary analysis determined the initial design parameters, leading to the selection of a rotary dryer for banana waste drying, with main assembly and 3D CAD simulation generated [21], [22]. Utilizing 3D CAD tools, the preliminary design was developed, followed by optimization of flight designs to enhance drying efficiency [23]. Analytical input parameters, including Biot number and incremental specific heats, played a crucial role in determining the optimal dryer diameter and length.

To validate the design, simulation techniques such as Design of Experiments (DoE) were employed.

This validation process ensured consistency between the 3D CAD model and analytical results, as depicted in Figure 1. Specifically, the Biot number was employed in the analysis of drying time, and incremental specific heats were utilized in forced heat and mass transfer calculations to ascertain the optimal dryer diameter. Subsequently, this determined the diameter, along with the established drying time, is incorporated into the residence time equation to derive the appropriate length of the dryer.

To consolidate all the obtained data and validate the overall dryer design, scenario analysis was conducted from the results of Design of Experiments (DoE) and calculations. This comprehensive approach ensured alignment and coherence across the analytical, numerical, and simulation aspects of the rotary dryer design, as illustrated in Figure 1.
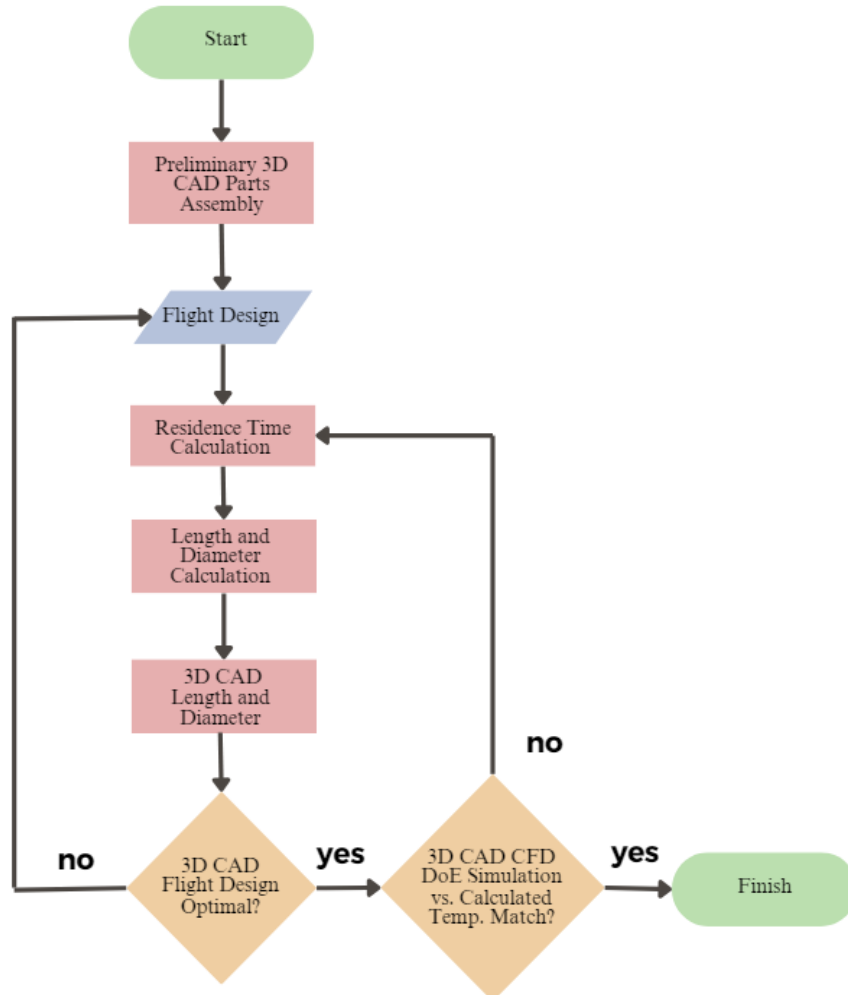

Figure 1. Banana waste rotary dryer 3D CAD design and simulation process model

2.1. Preliminary Parts, Subassemblies and Main Assembly using 3D CAD

The illustration drawings of various parts, subassemblies and main assembly were 3D drawn using CAD. This was done to aid in envisioning the design of the rotary dryer. There were numerous parts drawn. Once the parts drawings were completed, they were put together to comprise the nine (9) subassemblies. Thereafter completion of all the nine (9) subassemblies, they were assembled to form the main assembly or the complete unit of the rotary dryer. Figure 2 illustrated the main assembly design of the rotary dryer, with numerical labels 1, 2, 3, 4, 5, 6, 7, 8, and 9 indicating the locations of the nine subassemblies.
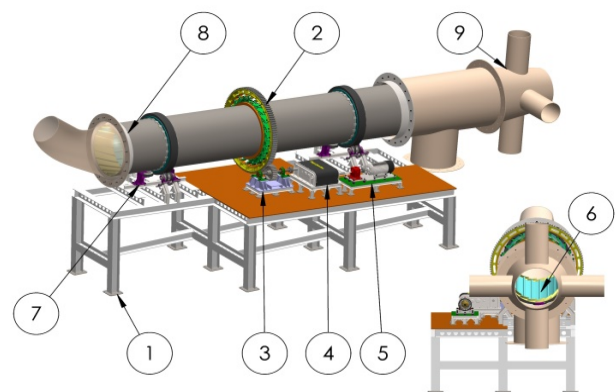

Figure 2. Main assembly design of rotary dryer

Table 1 listed the nine subassemblies that constituted part of the main assembly, along with their respective functions.

Table 1. List of the rotary dryer's subassemblies

Item Number	Part Name	Function	Quantity
1	Dryer platform subassembly	Supports the drum and its sub-components	1
2	Gear-flange subassembly	Holds the drum and link the mechanism to the drive	1
3	Drive gear-bearing subassembly	Provides rolling guides of the drum	1
4	Gear box-transmission subassembly	Controls the speed ratio of the gear	1
5	Motor subassembly	Provides rotating motion of the drum	1
6	Flights subassembly	Provides dispersion and cascading effects of material	1
7	Roller subassembly support frame	Mounts and supports the roller assembly	2
8	Feed chute subassembly	Provides material entry point	1
9	Out-chute subassembly	Provides exit point of the dried material	1

In Figure 3, the dryer platform subassembly was depicted as item 1, while Figure 4 showed the gear-flange subassembly as item 2. Similarly, Figure 5 displayed the drive gear-bearing assembly as item 3, and Figure 6 showcased the gear box-transmission subassembly as item 4.

ITEM NO.	PART NAME	QTY.
1	long bed element 1	2
2	short bed element 2	16
3	vertical leg 1	2
4	vertical leg 2	3
5	vertical leg 3	3
6	vertical leg 4	3
7	horizontal leg 1	5
8	base plate	11
9	horizontal bed	1
10	horizontal bed extension	1
11	table plate	1
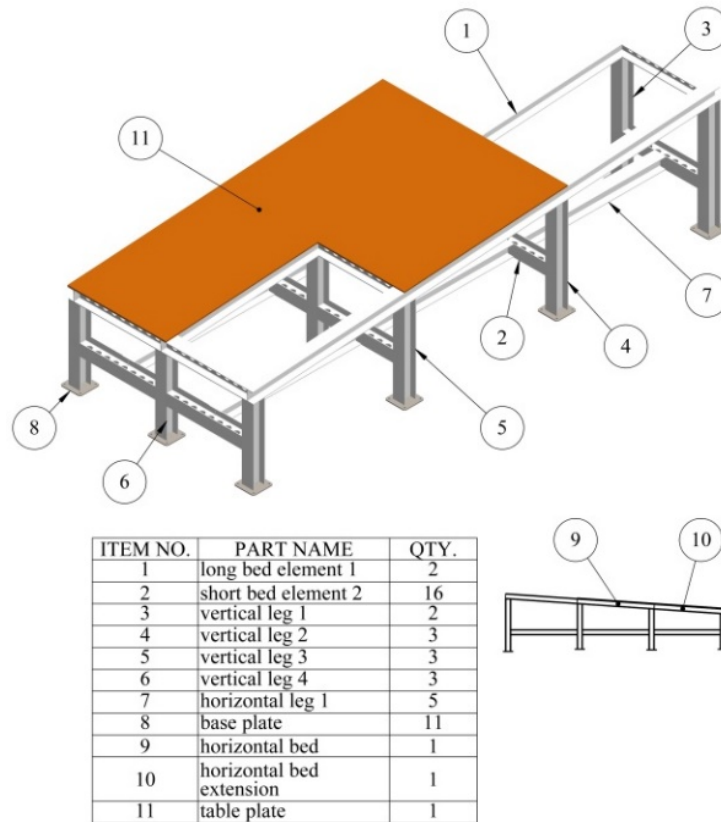
Figure 3. Dryer platform subassembly
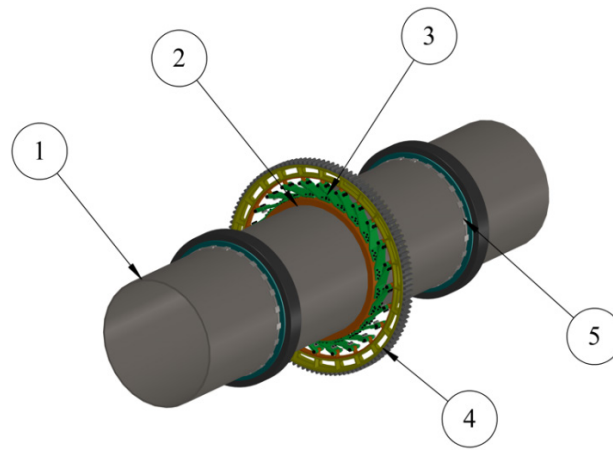
ITEM NO.	PART NAME	QTY.
1	drum	1
2	gear base	1
3	flange assembly	24
4	gear hub assembly	1
5	roller guide ring	2

Figure 4. Gear flange subassembly
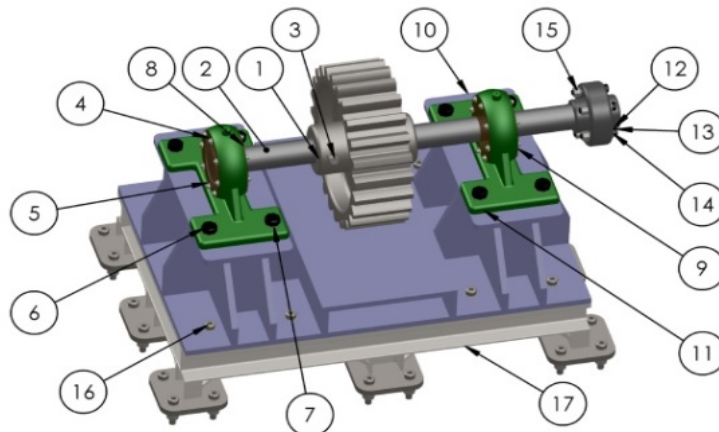
ITEM NO.	PART NAME	QTY.
1	spur gear	1
2	spur gear shaft	1
3	M15X70 hex cap screw	2
4	thrust bearing	2
5	bearing end casing	2
6	M20X60 bolt	8
7	M20 washer	8
8	cover shaft assembly	2
9	bearing cap assembly	2
10	mounting table	1
11	M20 nut	8
12	shaft joint connector	2
13	M12X70 bolt	5
14	M12X27 washer	5
15	M12 nut	5
16	M15 screw washer assembly	10
17	drive gear stand channel assembly	1

Figure 5. Drive gear-bearing subassembly

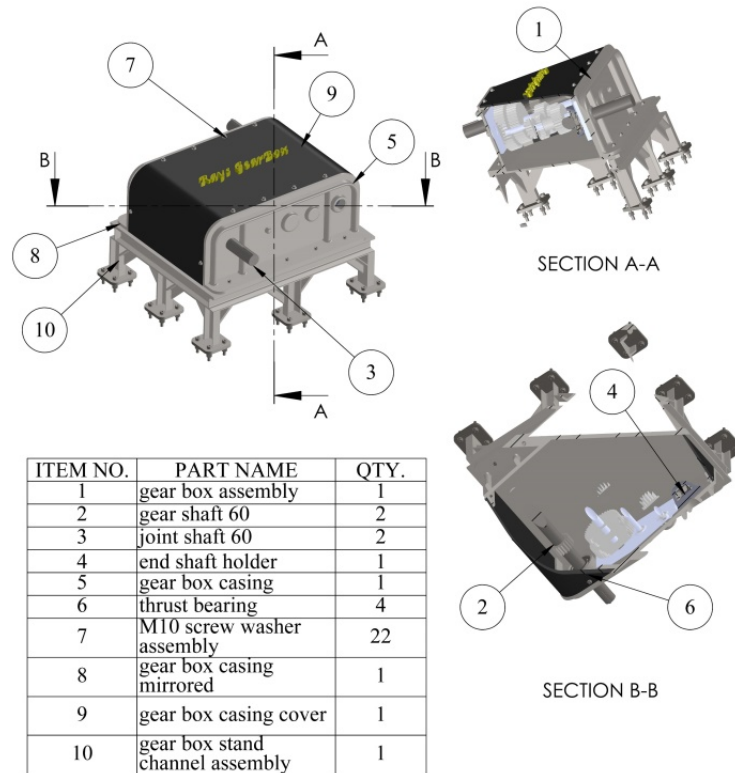| ITEM NO.	PART NAME	QTY.
1	gear box assembly	1
2	gear shaft 60	2
3	joint shaft 60	2
4	end shaft holder	1
5	gear box casing	1
6	thrust bearing	4
7	M10 screw washer assembly	22
8	gear box casing mirrored	1
9	gear box casing cover	1
10	gear box stand channel assembly	1

Figure 6. Gear box-transmission subassembly

The commencement of this phase involved the creation of detailed part drawings, encompassing a diverse array of components essential to the structural integrity of the rotary dryer. Once these individual part drawings were finalized, a systematic integration process followed, resulting in the formation of nine distinct subassemblies. Each subassembly constituted a cohesive grouping of interconnected parts and components, contributing synergistically to the overall functionality of the dryer.

Upon the completion of all nine subassemblies, the subsequent phase involved the careful and meticulous assembly of these subunits to constitute the main assembly. This main assembly represented the holistic and fully integrated unit of the rotary dryer. In essence, this methodical progression facilitated a comprehensive transition from individual components to subassemblies and, ultimately, to the fully realized main assembly of the rotary dryer.
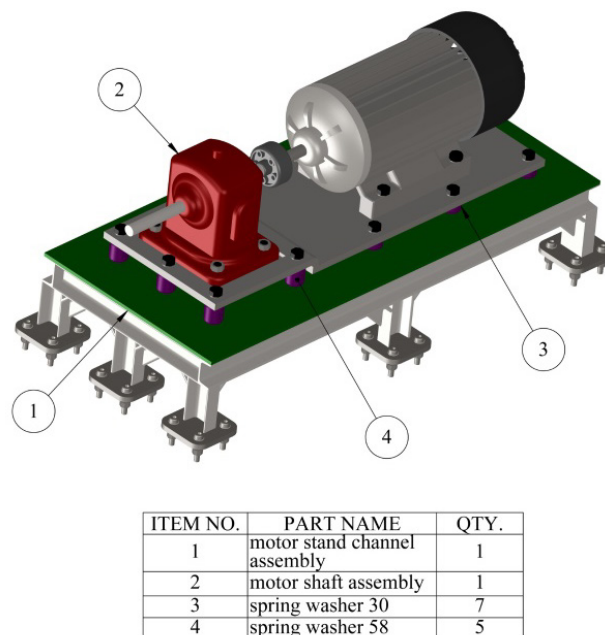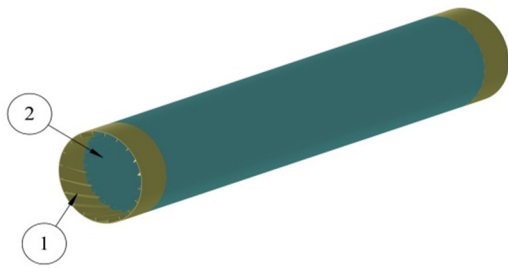

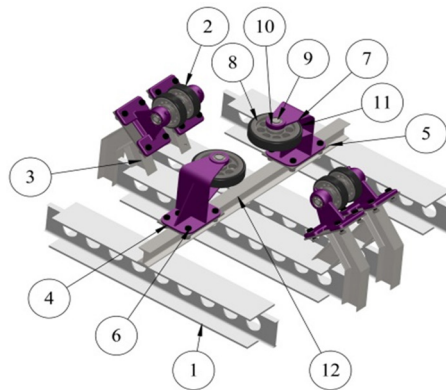| ITEM NO.	PART NAME	QTY.
1	motor stand channel assembly	1
2	motor shaft assembly	1
3	spring washer 30	7
4	spring washer 58	5

Figure 7. Motor subassembly

Specific subassemblies were visually delineated in the drawings, providing clarity to the overall design. For example, Figure 7 showed the motor subassembly as item 5, and Figure 8 depicted the flight assembly as item 6.

Furthermore, Figure 9 presented the roller subassembly support frame as item 7, and Figure 10 illustrated the feed-chute subassembly as item 8. Finally, Figure 11 provided an illustration of the out-chute assembly as item 9.
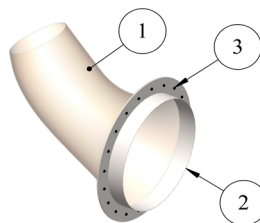

ITEM NO.	PART NAME	QTY.
1	spiral flights	2
2	revised semicircular flights	1

Figure 8. Flights subassembly

ITEM NO.	PART NAME	QTY.
1	short bed element 2	4
2	roller assembly	2
3	roller bearing support 1	4
4	side roller assembly	1
5	side roller bearing plate	2
6	M20X60 bolt washer assembly	8
7	side roller bearing casing	1
8	side roller wheel	1
9	side roller shaft	1
10	thrust bearing	2
11	side roller	1
12	side roller bearing support	1

Figure 9. Roller subassembly support frame

ITEM NO.	PART NAME	QTY.
1	feed chute in	1
2	feed chute in flange	1
3	M20X60 screw washer assembly	20

Figure 10. Feed chute subassembly
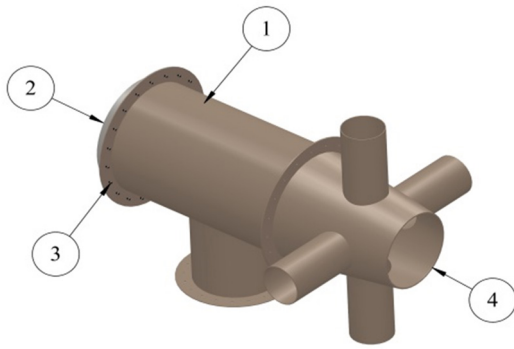
ITEM NO.	PART NAME	QTY.
1	feed chute out	1
2	feed chute out flange	1
3	M20X60 screw washer assembly	20
4	burner duct	1

Figure 11. Out-chute subassembly

CAD was used all throughout in 3D illustration drawings. Foregoing figures provided a closer detail of how subassemblies interact with other subassemblies whereby Figure 12 depicted how gear flange, drive-gear bearing, and gear-box transmission subassemblies were combined, while Figure 13 showed drum and roller assembly support frame illustration and assembly drawing. Figure 14 exhibited the left-side perspective view illustration drawing of the main assembly, offering a comprehensive understanding of the integrated system.
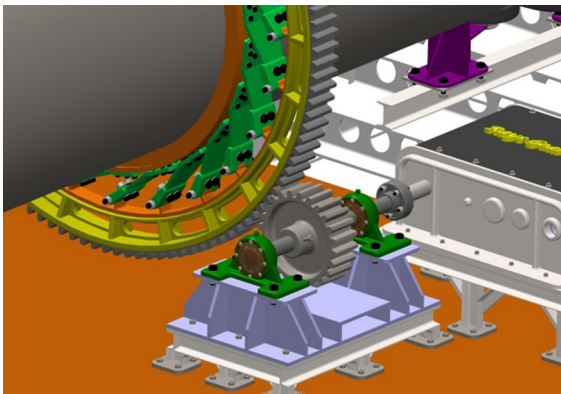

Figure 12. Gear-flange assembly, drive-gear bearing assembly and gear-box transmission assembly in illustration assembly drawing

The illustration drawing designs were intended to give an idea to the manufacturer, supplier, or vendor about what the client wants from a service or product. The purpose of the drawing was to illustrate each part, the sub-assemblies, and the main assembly. This enabled the generation Bill of Materials (BOM). Contained within the bill of materials were critical details such as part names, part numbers, quantities, specifications, and comprehensive descriptions.

This thorough document played a central role in steering the manufacturing process, ensuring the accurate production of each component in the required quantities.
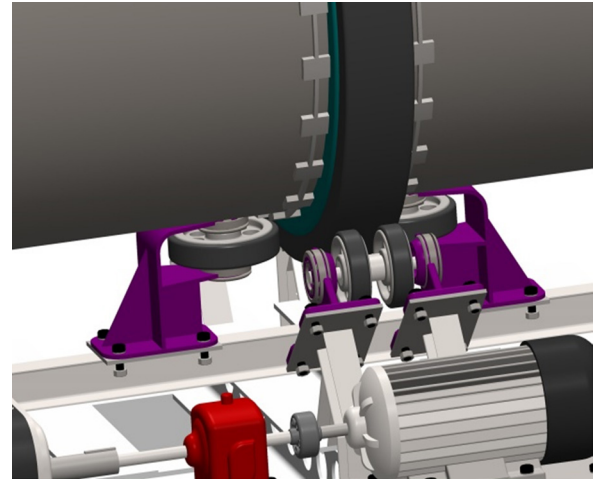

Figure 13. Drum and roller assembly support frame illustration and assembly drawing
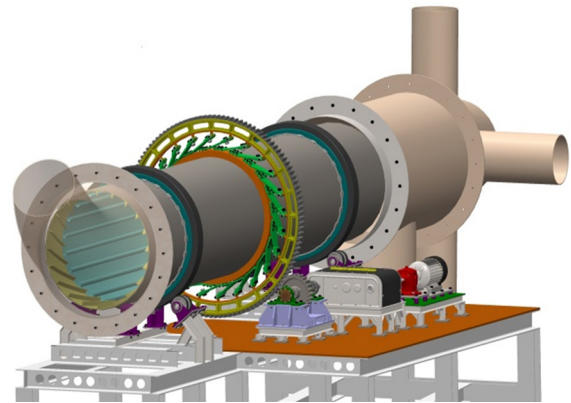

Figure 14. Left side perspective view illustration drawing

On one end, the manufacturing of individual parts was often based on the parts drawings which will include thorough details on the dimensions, material, quantity, machine process, scale, and other fabrication- related information. Subsequently, the working drawings, incorporating all essential information and dimensions, were printed on standardized templates or sheets. These working drawings served as indispensable guides for fabricators or suppliers, furnishing them with precise instructions for producing each component according to specified requirements. The working drawings for the designed dryer were shown below. Figure 15 and Figure 16 featured the working drawings for the designed dryer, showcasing specific parts such as the circular gear flange and the shaft casing. These drawings provided in-depth insights into the design, enabling fabricators to interpret and execute the manufacturing process with precision.
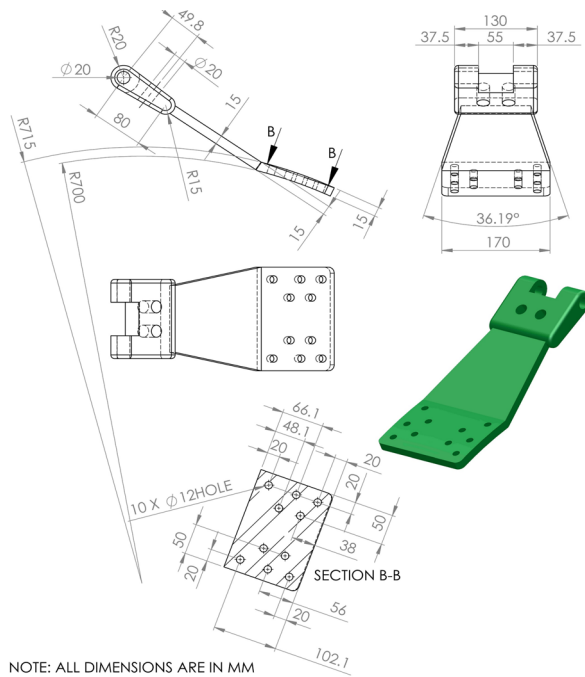
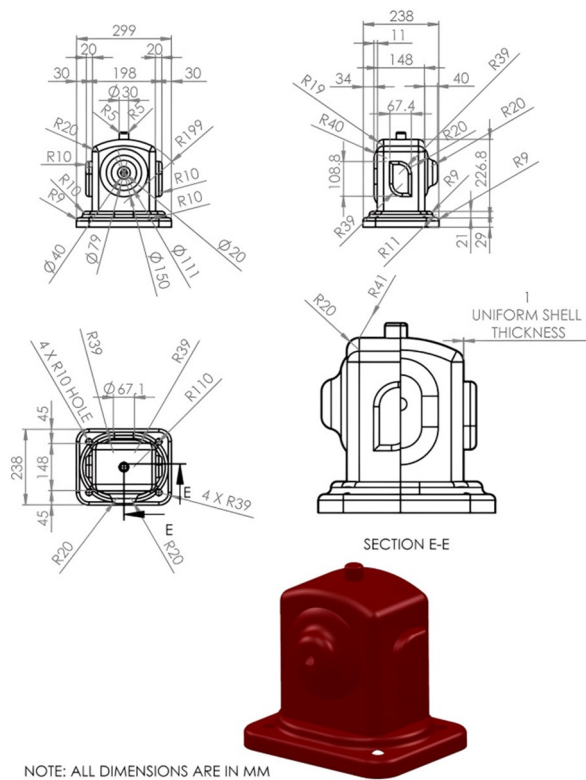*Figure 15. Circular gear flange part drawing*

Figure 16. Shaft casing part drawing

Working drawings played a crucial role in guiding the actual production of components by providing detailed dimensions, material specifications, and fabrication processes. Their meticulous detailing ensured precision, contributing to the creation of accurate and consistent parts. Standard templates enforced a consistent format, aiding quality control and promoting efficient collaboration. The combined effect between illustration and working drawings

facilitated the seamless translation of design concepts into functional components. The iterative process allowed for feedback from fabricators, addressing manufacturability and cost-effectiveness. These drawings served as comprehensive documentation, providing traceability, and recording modifications. Combining illustration and working drawings enhanced production efficiency, enabling fabricators to proceed confidently with clear instructions.

2.2. Optimal Flight Design

The identification of holdup regions in rotary dryer flights was conducted using 3D CAD design limitations, with the sum of these regions serving as a basis for assessing dryer performance efficiency. This aimed to ensure that the dryer's holdup volume fell within the benchmark range of 10 to 15 percent of the overall volume [24]. 3D CAD was utilized to optimize flight designs, their numbers, and holdup volume, aiding in the selection of the optimal flight design. Calculations of holdup volumes for each flight design and various flight numbers were performed using 3D CAD, complemented by experiments involving different flight designs to determine the most effective configurations for material retention within the drum [24]. A study mentioned in Fernandes *et al.* [13] of Equation (1) represented a correlation between the dynamic angle of repose (ϕ) and the dynamic coefficient of friction (μ) of the powder material, the angular position (θ) of the tip, the radial position (R_0) of the flight tip, and the rotation speed of the drum shown in Equation (1). This equation was developed from an equilibrium balance of the forces acting on a particle that is going to drop from a flight.

$$tan\,\theta = \frac{\mu + R_0\frac{\omega^2}{g}(cos\theta - \mu sin\theta)}{1 - R_0\frac{\omega^2}{g}(sin\theta - \mu cos\theta)} \qquad (1)$$
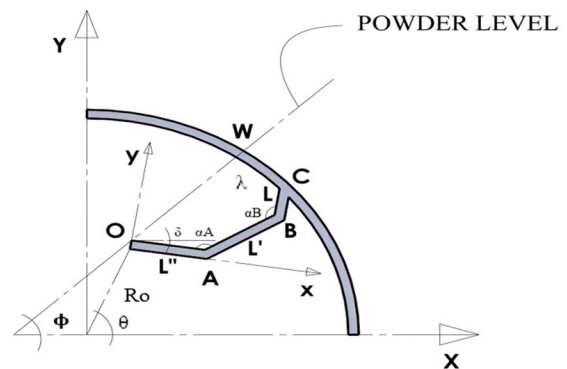

Figure 17. Scheme of 3-segment flights with main dimensions and Scheme of 3-segment flights with main dimensions and variables used in the equation

The three-segment type of lengths *L, L′*, and *L″*; their angles αA and αB, and the radius R_0 of the circle formed by the flying tip O as the drum rotates were used to describe the flight in Figure 17, considering the two sets of Cartesian coordinates [13]. The (x, y) set origin was at the tip of the flight, and its axis ran along the first segment. As the flight rotated, this set of coordinates moved. The drum axis served as the origin of the stationary (X, Y) set, with the X-axis being horizontal.

According to Mujumdar [24], the flights in Figure 18 (a, b, c, and d) were widely utilized in cascading rotary dryers; while Figure 18 (a), on the other hand, was appropriate for sticky substances in the dryer's wet end; and Figure 18 (c), which is semi-circular in shape, was used as an alternative to types b and d because it was thought to be simpler to produce. Flights with EAD (equally angled distribution) and CBD (centrally biased distribution) had been proposed to enhance dryer performance, but their profiles were intricate.
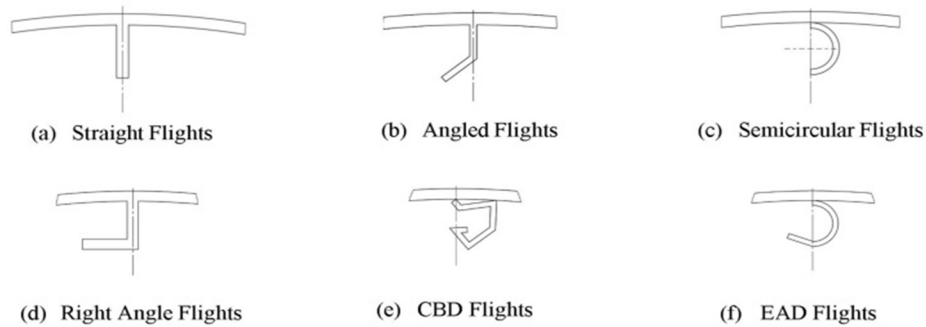

Figure 18. Different flight profile

2.3. Residence Time Calculation

The equipment for drying had been systematically classified into various categories, a crucial step in selecting the most suitable dryer for a given task and comprehending the underlying principles governing its operation. The key classification parameters included feed and product form (solid or liquid, sheet, or slab), operation mode (batch or continuous), heat transfer mode (convective (direct), conductive (indirect), radiative, or dielectric), solid condition (static bed, moving bed, fluidized, or dispersed), gas-solids contacting (parallel flow, perpendicular flow, or through-circulation), and gas flow pattern (cross-flow, co-current, or countercurrent).

Table 2. Dryer selection guide and material properties

Information on Dryer	
Factors	Selection Remarks
Dryer type	Rotary
Mode of operation	Continuous
Mode of heat transfer	Convective and direct
Condition of solids	Moving and dispersed
Gas-solids contacting	Through-circulation
Gas flow pattern	Countercurrent
Feed rate	1-5 ton per hour
Additional post and after drying equipment	Presser, Shredder, Siever

Initial Material Information	
Factors	Selection Remarks
Material	Banana solid waste (pseudo stem, leaves, and peelings)
Form of feed	Wet solid
Material shape	Particulate after pressing, shredding, and sieving process
Initial particle size	15 to 25 mm rectangular with 5mm thickness (proposed in this study for rotary dryer)
Final particle size	Uniform size
Initial moisture content	Banana stem 90.75%, Banana peels 84.5%
Final moisture content	10% below
Shrinkage	Not severe
Density	Banana stem $1231.367\,kg/m^3$, avg.
Thermal conductivity	Banana fiber $0.04415\frac{W}{m^2 \cdot K}$ at $70.4\frac{kg}{m^3}$
Specific heat of solid	1.76 kJ/kg °C dried
Stickiness, lumping, caking (wet)	Not severe
Type of moisture	Unbound
Initial temperature	T_{m1} or $T_i = 30°C$, varies with local climate
Dryer temperature at inlet	T_∞ or $T_2 = 145°C$
Temperature at center	$T_{m2} \geq T_{center} = 100°C$ at falling rate drying period
Combined heat transfer coefficient	$h_{combined} = 120\frac{W}{m^2 \cdot K}$ a range from 10-500 for forced convection

In Table 2, comprehensive details regarding the selection of rotary dryers and specific information related to banana waste materials were provided. This holistic classification approach aimed to facilitate informed decision-making in choosing the most suitable dryer configuration based on the unique requirements of the material and the desired drying outcomes.

In a rotary dryer, residence time 't' needed to be aligned with the required drying time. It held common that heat transport often involves one-dimensional flow, but multi-dimensional heat conduction can occur. Classification factors included steady or transient heat conduction. Lumped system analysis, modeling certain bodies as a "lump," involved studying heat transfer using Newton's law of cooling and a derived first-order differential equation, represented by Equation (2).

time 't' needed to be aligned with the required drying time. It held common that heat transport often involves one-dimensional flow, but multi-dimensional heat conduction can occur. Classification factors included steady or transient heat conduction. Lumped system analysis, modeling certain bodies as a "lump," involved studying heat transfer using Newton's law of cooling and a derived first-order differential equation, represented by Equation (2).

$$ln\frac{T(t)\text{-}T_\infty}{T_i\text{-}T_\infty} = \frac{hA_s}{\rho V C_p} \qquad (2)$$

By substituting the body's specific heat capacity into the heat conduction equation, the equation transformed into Equation (3), was known as Biot

$$Bi = \frac{hA_s}{kt\frac{A_s}{L}b} = \frac{hL}{k} \qquad (3)$$

number, denoted as Bi, represents the ratio of surface heat convection to internal heat conduction, quantifying their relationship. Higher convection coefficients had resulted in rapid temperature decreases near the body's surface. The Biot number governed the extent of maximum temperature difference within a body during heat transfer. Equation (4) combined Fourier's and Biot's principles for transient one-dimensional heat conduction in the x-direction without heat generation [20].

$$\frac{\partial^2 T}{\partial x^2} = \frac{1}{\alpha}\frac{\partial T}{\partial t} \qquad (4)$$

where $\alpha = \frac{k}{\rho c}$ was the thermal diffusivity of the material.

The precision of lumped system analysis improves with a lower Biot number, typically deemed appropriate when Biot ≦ 0.1. Beyond this, a more straightforward solution, expressed in Equation (5) for the one-term approximation method, was considered applicable, especially for the center of a plane wall at x equals zero. The infinite series solution was noted to be particularly useful for complex one-dimensional transient heat conduction problems [20].

$$\theta(x,t)_{wall} = \frac{T(x,t)\text{-}T_\infty}{T_i - T_\infty} = A_1 e^{-\lambda_1^2 \tau} cos(\lambda_1 x/L) \qquad (5)$$

The one-term approximation method became advantageous as the terms in the solutions converge rapidly with increasing time. Notably, for the dimensionless time quantity, or Fourier number, denoted as $\tau = \alpha t / L^2$, when τ is greater than 0.2, retaining only the first term while neglecting the subsequent terms in the series resulted in an error of less than 2% [20].
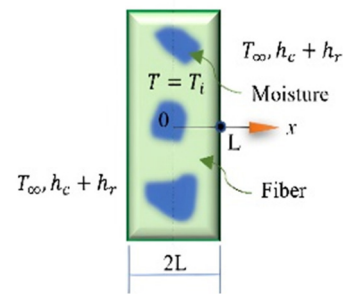
Figure 19. Banana stem particulate geometry
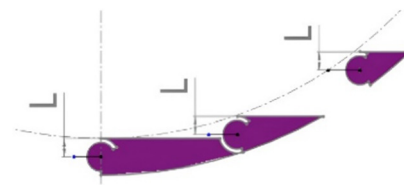
Figure 20. Holdup volume material in flights inside dryer

This practical approach provided an efficient means of approximating solutions, ensuring a balance between accuracy and computational simplicity in analyzing heat conduction problems. Figure 19 illustrated a one-dimensional model of banana stem particulate, including parameter properties for computing drying time results. Figure 20 indicated the geometry for the one-term approximation method.

2.4. Diameter and Length Calculation

The drum's desired diameter was determined through numerical modeling of heat and mass transfer in the material.

This involved considering incremental sensible and latent heat, and the equation derived from Newton's law of cooling. The system was assumed to move steadily through the dryer at a constant speed, with unrestricted air flow in one direction along the drum's length. The rotary dryer's diameter was computed using equations from Mujumdar [24], following a design process. Five distinct operations required specific amounts of heat to remove water from the substance.

The vapor was heated from the initial wet-bulb air temperature to the hot air exit temperature. To facilitate water evaporation, heat was applied to raise its initial temperature upon entering the dryer to the air's inlet wet bulb temperature. The dry solid underwent heating from the entrance temperature to the exit temperature of the dryer. The water remaining in the finished product was heated to increase its temperature from the material's inlet to its exit.

A correlation was estimated to determine the total heat delivered to the product, accounting for heat losses due to radiation and, particularly, conduction between the dryer's exterior and the surrounding air. Mujumdar [24] indicated that these losses amounted to approximately 7.5–10% of the heat consumption provided the ratio of heat for evaporation describes the process of evaporating moisture content, which used the most heat.

The total heat calculation process was used to determine the required air mass rate for effective heat transmission during drying. The highest air temperature, denoted as T_1, and the specific heat of air (in $kJ/kg \cdot °C$), represented as $C_{p, air}$, were integral to the calculation. The researchers introduced a definition for the number of heat transfer units (NT) while computing the heating of the airstream from the initial atmospheric temperature, $T_0 (°C)$, to the input air temperature of the dryer, T_1. The thermal efficiency of the dryer was subsequently determined, leading to the calculation of the cylindrical shell's diameter using Equation (6).

$$D = \sqrt{\frac{4G}{3600\,\pi\,j\,u}} \qquad (6)$$

Two critical considerations were held essential in estimating the dryer's diameter (in meters). Firstly, it had to be sufficiently large to prevent the air mass velocity (in $kg/m^2 s$) from exceeding levels that could cause entrainment of the product. Secondly, the assumption that only a portion of the dryer's cross-section was open to the air was crucial, as it dictated the amount of air that could pass through freely. Operational insights from rotary dryers indicated that the proportion was approximately 85% (j = 0.85).

The length of the rotary dryer was determined through calculations based on volume holdup, diameter, residence time, and feed rate at intake on a wet basis. The density utilized for these computations represented the average ratio of banana stem containing the initial material moisture content. Additionally, the use of the feed rate on a wet basis at the exit was deemed acceptable, provided it was coupled with the appropriate density value. Linear velocity along the length of the dryer was calculated by employing volume holdup, density, and feed rate.

3. Results and Discussion

This part aimed to provide the results and the detailed discussion of 3D CAD flight, residence time, diameter and length calculation, design of experiments, and simulation.

3.1. 3D CAD Fight Design Results

Based on 3D CAD simulation and the summary of tabulated results in Table 3 with an effective diameter of 1.103345 m and a 2 m length initially considered dimensions, whereby, the researchers selected the CBD flights at $nf = 11$ as the number of flights, where the volume was $0.0718517\ m^3$, which was higher than straight flights, angled flights, semi-circular flights, and EAD flights. The CBD flights exhibited a broader material drop distribution compared to EAD (equal angle distribution) and right-angled flights. Additionally, the CBD flights demonstrated a higher material hold-up ratio than semi-circular flights. However, adherence to the geometrical restrictions outlined by Mujumdar [24] suggested a limit of $6.56 \leq \left(\frac{nf}{D}\right) \leq 9.84$ indicating that, depending on the drum diameter, the number of flights might fall out of the acceptable range. Nevertheless, adjustments and revisions were facilitated using 3D CAD. Furthermore, considering the guideline of 5% < H/V < 15%, the material hold-up ratio for CBD flights was 3.18%, falling outside the acceptable range. However, it was noted that by decreasing the effective diameter, this ratio could be brought within the normal range.

Table 3. Volume of material holdup initially at 1.2 m inner diameter, 1.106345 m effective diameter, and 2 m length for various flight designs using 3D CAD

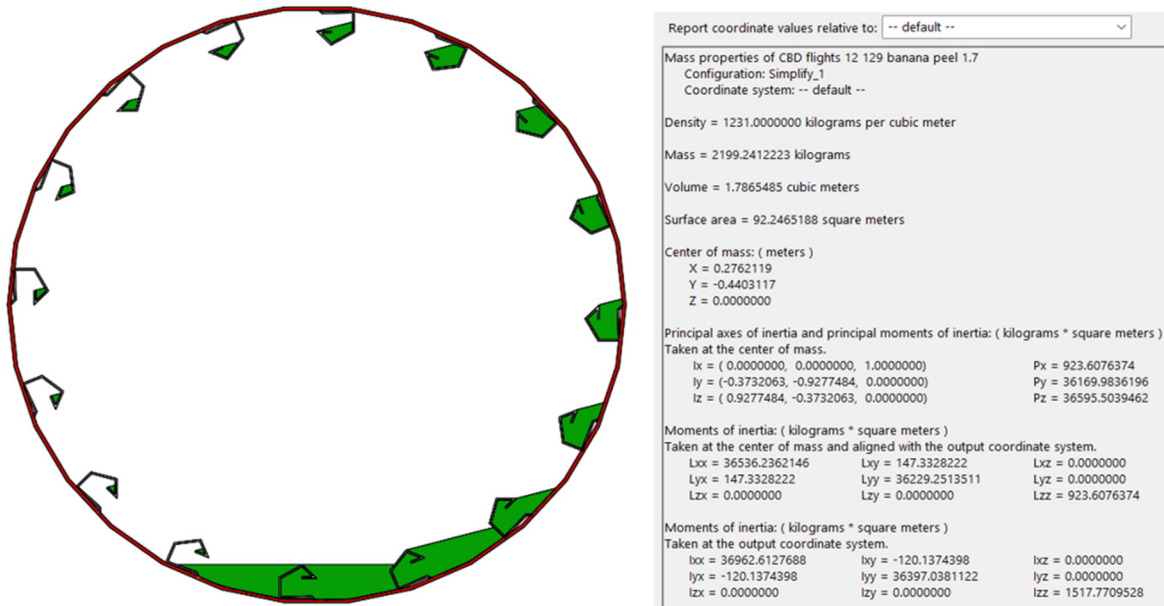| Types of Flights	$nf = 11,\ m^3$	5%<H/V<15%
Straight flights	0.0573634	2.54%
Angled flights	0.0564515	2.50%
Semi-circular flights	0.0620932	2.75%
Right angled flights	0.068835	3.04%
EAD (equal angle distribution flights)	0.066126	2.92%
CBD (centrally biased distribution flights)	0.0718517	3.18%

Figure 21. Simulated material hold up of CBD flights at nf=16

With a density of 1231.00 kg/m^3, a mass of 2199.2412223 kg, a volume of 1.7865485 m^3, and a surface area of 92.2465188 m^2 in contact with heat, Figure 21 clearly illustrated the simulated material hold up of CBD flights at nf=16.

Applying CBD flights in this dryer, the calculated diameter was determined at 1.75394 meters, and the calculated length at 14.0034 meters. With 16 flights, the ratio (nf / D) is calculated as 9.1223189, which was within the specified range limit of $6.56 \leq \left(\frac{nf}{D}\right) \leq 9.8$. Additionally, the material hold-up to dryer volume ratio was within the acceptable limit at 5.282 %. These results adhered to the defined design constraints and criteria as shown in Table 4.

Table 4. Volume of material holdup at calculated 1.75394 m inner diameter and 14.0034 m length at effective diameter using CBD flights

	Volume of material hold up, nf=16, m^3	Effective diameter, m	5%<H/V<15%
CBD (centrally biased distribution flights) based on residence time calculation	1.7865485	1.53794	5.282 %

The 3D CAD simulation results were systematically optimized, aiming to achieve maximum volume hold-up within the constraints of an appropriate limit on the number of flights.

3.2. Residence Time Results

The simulated outcomes utilizing the one-term approximation method in a lumped system revealed an optimal half-thickness (L) of 5.4 cm for banana stem particulate with 90.75% moisture, corresponding to a drying time of 62 minutes. The simulated temperature at the banana stem center was 100 degrees Celsius, with an inlet air temperature of 145 degrees Celsius. These results suggested valuable insights into the drying process, aiding in the identification of optimal conditions for drying banana stem particulate with specific moisture content.

3.3. Diameter and Length Calculation Results

The researchers outlined input and output parameters, summarizing results in Table 5 to indicate the rotary dryer's performance across varying thermal efficiency and temperature conditions. Calculations yielded a rotary dryer diameter of 1.75394 and a corresponding length of 14.0034. The number of heat transfer units was within the 1.5-2.5 range at 1.51871, with an air exit temperature of 98 °C. Thermal efficiency was within the 55-75% range at 58.315, and the system was designed to utilize flue gas as a potential heat source. Optimal performance aligned with the set condition of 4<L/D<10, which in this case was 7.983967. Considerations for length involved gravity, drum rotational speed, tilting angle, drag, and other influencing factors.

Parameter	Experiment 1	Calculated 1	Experiment 2	Calculated 2	Experiment 3	Calculated 3	Experiment 4	Calculated 4	Experiment 5	Calculated 5
Mass flux (Inlet Mass Flux 1) [kg/(s*m^2)]	4.25	4.25	3.75	3.75	4.5	4.5	4	4	3.5	3.5
Point 1										
Temperature (Fluid) [K]	374.7069526	374	373.5296646	369	375.2426856	373	374.1512334	371	372.87509	369
Temperature (Solid) [K]	310.7970365	312	309.1594068	314	311.6708564	309	309.9498657	303	308.267999	316
Point 28										
Temperature (Fluid) [K]	415.3124404	417	415.2064202	417	415.3199978	414	415.2596214	418	415.1244502	420
Temperature (Solid) [K]	326.0491443	324	324.2327167	322	326.7160809	324	325.1903885	323	323.2640039	321
Medium	Fluid/Solid		Fluid/Solid		Fluid/Solid		Fluid/Solid		Fluid/Solid	
x [m]	-0.578432739		-0.578432739		-0.578432739		-0.578432739		-0.578432739	
y [m]	-0.513037026		-0.513037026		-0.513037026		-0.513037026		-0.513037026	
z [m]	13.79409981		13.79409981		13.79409981		13.79409981		13.79409981	

	%error	%error	%error	%error	%error	
Temperature (Fluid) [K]	0.189024753	1.227551388	0.60125619	0.849389067	1.050159904	0.783476261
Temperature (Solid) [K]	0.385565225	1.541590183	0.864354822	2.293685044	2.446835766	1.506406208
Temperature (Fluid) [K]	0.404690563	0.430115049	0.318840038	0.655592955	1.160845201	0.594016761
Temperature (Solid) [K]	0.632451958	0.693390278	0.838296571	0.678138864	0.705297175	0.709514969
Ave. error	0.402933125	0.973161725	0.655686905	1.119201483	1.340784511	0.89835355
						99.10164645

Figure 22. Design of Experiments with five scenarios and calculations

Table 5. Process design calculations for the diameter of the dryer

Input parameters		Value	Remarks
Overall inlet material	F_1	1182.65 kg/hr	1–5-ton capacity wet feed, Simulation
Specific heat of air	$C_{p,ai}$	1.06198 kJ/kg	At avg. temp.
Specific heat of vapor	C_{pv}	1.04892 kJ/kg	At avg. temp.
Specific heat of water	C_{pw}	4.178 kJ/kg·K	At avg. temp.
Air exit temperature	T_2	98 °C	High temp. chart[1]
Material temperature at exit	T_{m2}	50°C	High temp. chart[1]
terial exit moisture	X	0.1%	average
Heat loss	H_l	0.1%	average
Air mass velocity	u	4 kg/m²·s	3-5
Residence Time		62 min	calculated
Output parameters		Result	Remarks
Flow rate of material	F_1	1182.65	calculated
Overall exit material	F_2	682 kg/hr	calculated
Evaporating water	m_{ws}	500.65 kg/h	calculated
Heat for evaporation	Q_1	1176527.5	calculated
Heat for vapor	Q_2	6964.43	calculated
Heat for liquid	Q_3	113789	calculated
Heat for product solid	Q_4	49100	calculated
Heat for product water	Q_5	5180.72	calculated
Overall heat consumption	Q_T	1486718	calculated
Number of heat transfer units	N_T	1.51939	1.5-2.5
Air mass rate	G	29573.5 kg	calculated
Heat load of exchanger	Q_{he}	2355483	calculated
Thermal efficiency	n_{th}	61.487 %	55-75%
Diameter	D	1.75394 m	calculated
Dryer Length	L_D	14.0034 m	calculated

[1]*Referring to high-temperature psychrometric chart*

3.4. Design of Experiments (DOE) and Simulation Results

By utilizing probe point parameters and incorporating the results into a 3D CAD simulation, the fluid air temperature, and the solid temperature on the surface of the banana stem were measured at the exit-side pick point parameters. The same pick point parameters for fluid and solid temperatures were measured at the inlet side of the drum. There were 28 pick point locations inside the drum dryer. Figure 22 compared the values obtained at the exit for waste banana stem and air temperatures during point parameter verification, subsequently employed in the DoE. These values were considered reliable and comparable results from the computations were obtained. A total of five experimental scenarios were provided by the DoE, featuring temperature values at different pick point locations inside the drum. Pick points 1 and 28 were selected as they represent the inlet and exit points of the material inside the drum. The flow of hot gas was on the opposite side. These carefully controlled conditions and air mass flux of 3.5, 3.75, 4, 4.25, and 4.5 were implemented and run to simulate experimental scenarios. In Figure 23, the visualization, and results of the simulation with particle study were depicted, showcasing cut plots with isolines representing the temperatures and velocities. Figure 24 illustrated the exponential graph of fluid and solid temperatures at an air mass flux of 4.
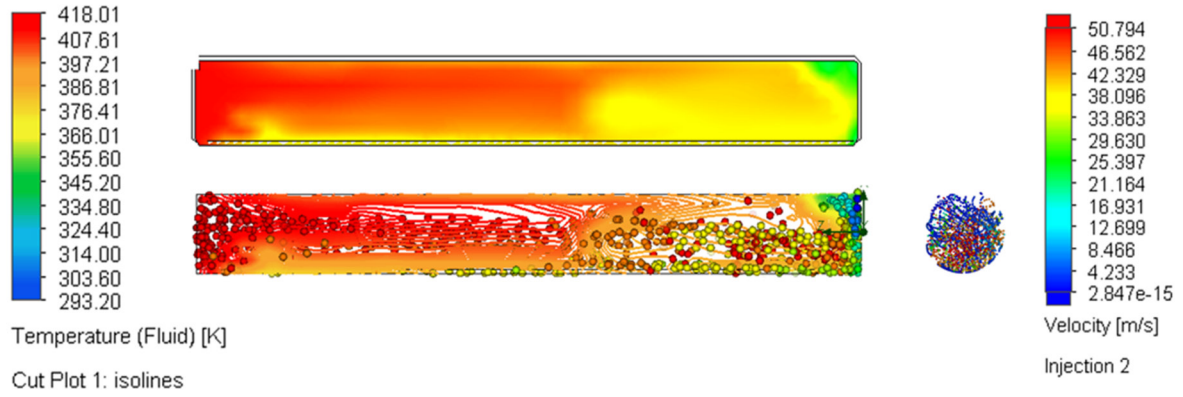
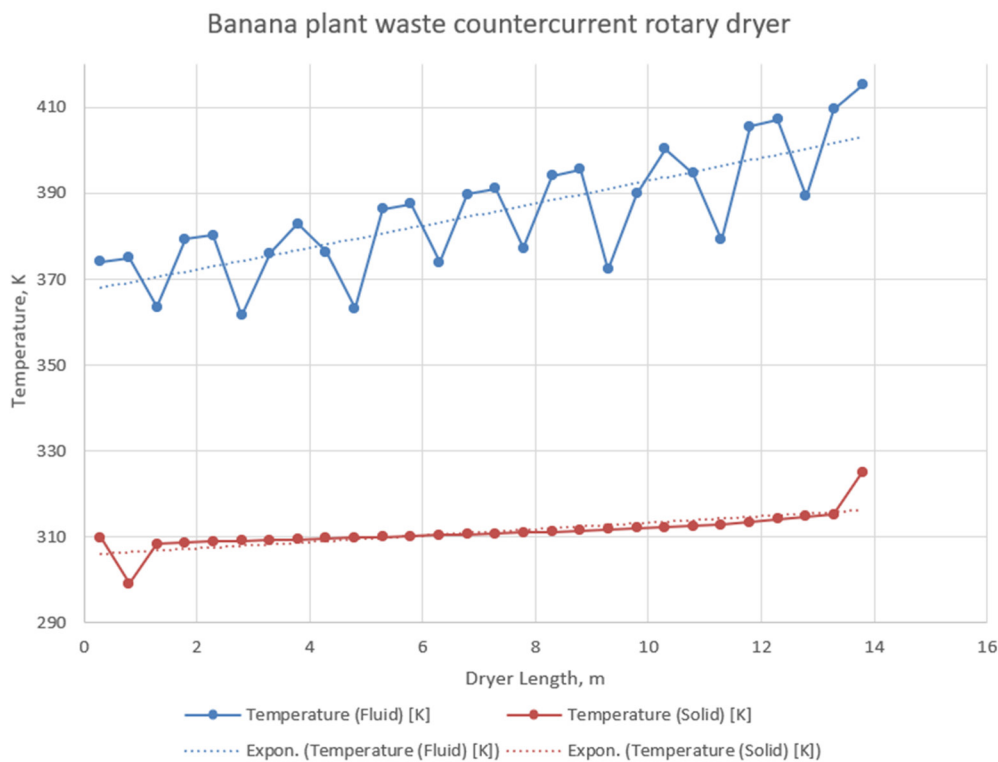*Figure 23. Temperature and velocity plots with particles and isolines*

Figure 24. Exponential graph of fluid and solid temperatures at air mass flux of 4

The average error rate in the fluid temperature at exit was 0.5940 %. The average error rate in the fluid temperature at the inlet was 0.7835 %. The average error rate in the solid temperature at the inlet was noted at 1.5064 %. The average error rate in the solid temperature at exit was 0.7095 %. The average total error rate was 0.898 %.

4. Conclusion

For selecting input parameters with precision in the design process of the banana waste rotary dryer, a model was developed.

The initial phase involved creating preliminary 3D CAD parts and assemblies, optimizing flight design in 3D CAD, calculating residence time, and subsequently determining the diameter and length, with Biot number playing an important role, and then verified by CFD simulation. The use of 3D CAD provided a quicker way to compute the volume of material hold-up in complex geometries. CFD Design of Experiments (DoE) and optimization procedures were employed to explore various scenario-driven outcomes and parameter-oriented goals, crucial in an environment where variables were continually changing for optimization.

The study found that the calculations were consistent with CFD simulation and the sets of DoE optimization scenarios.

The analysis revealed variations in error rates among different temperature points. Specifically, the solid temperature at the inlet exhibited the highest error rate, whereas the fluid temperature at the exit demonstrated the lowest error rate. Despite these variations, the overall average error rate in comparing the calculated fluid and solid temperatures with the simulated values was reported to be at 0.898 %, measured in units of degrees Kelvin.

References:

[1]. Olivares, B. O. et al. (2021). Fusarium wilt of bananas: A review of agro-environmental factors in the Venezuelan production system affecting its development. *Agronomy, 11*(5), 986. Doi:10.3390/agronomy11050986

[2]. Soares, J. M. et al. (2022). Gene expression, histology and histochemistry in the interaction between Musa sp. and Pseudocercospora fijiensis. *Plants, 11*(15), 1953. Doi:10.3390/plants11151953

[3]. Kuyu, C. G., & Tola, Y. B. (2018). Assessment of banana fruit handling practices and associated fungal pathogens in Jimma Town Market, Southwest Ethiopia. *Food Science & Nutrition, 6*(3), 609–616. Doi:10.1002/fsn3.591

[4]. Kumari, P., Gaur, S. S., & Tiwari, R. K. (2023). Banana and its by - products: A comprehensive review on its nutritional composition and pharmacological benefits. *eFood, 4*(5). Doi:10.1002/efd2.110

[5]. Vu, H. T., Scarlett, C. J., & Vuong, Q. V. (2018). Phenolic compounds within banana peel and their potential uses: A Review. *Journal of Functional Foods, 40*, 238–248. Doi:10.1016/j.jff.2017.11.006

[6]. Alzate Acevedo et al. (2021). Recovery of banana waste-loss from production and processing: A contribution to a circular economy. *Molecules, 26*(17), 5282. Doi:10.3390/molecules26175282.

[7]. Gueco, L. et al. (2020). Characterization and agronomic evaluation of naturally occurring short-statured Saba Banana in the Philippines. *Philippine Journal of Science, 149*. Doi:10.56899/149.3a.23

[8]. Despoudi, S. et al. (2021). Food Waste Management, valorization, and sustainability in the Food Industry. *Food Waste Recovery,* 3–19. Doi:10.1016/b978-0-12-820563-1.00008-1

[9]. Gupta, G., Baranwal, M., Saxena, S., & Reddy, M. S. (2022). Utilization of banana waste as a resource material for biofuels and other value-added products. *Biomass Conversion and Biorefinery, 13*(14), 12717–12736. Doi:10.1007/s13399-022-02306-6

[10]. Nirmal, N. P. et al (2023). Valorization of fruit waste for bioactive compounds and their applications in the Food Industry. *Foods, 12*(3), 556. Doi:10.3390/foods12030556

[11]. Hikal, W. M. et al. (2022). Banana peels: A waste treasure for human beings. *Evidence-Based Complementary and Alternative Medicine, 2022*, 1–9. Doi:10.1155/2022/7616452

[12]. Nguyen, M. R., & Tan, M. F. (2020). Solid waste management in urban and rural communities of Santa Cruz Watershed, Laguna, Philippines. *Pertanika Journal of Social Sciences and Humanities, 28*(4). Doi:10.47836/pjssh.28.4.20

[13]. Fernandes, N. J., Ataíde, C. H., & Barrozo, M. A. (2009). Modeling and experimental study of hydrodynamic and drying characteristics of an industrial rotary dryer. Brazilian Journal of Chemical Engineering, 26(2), 331–341. Doi:10.1590/s0104-66322009000200010

[14]. Ceryes, C. A. et al. (2021). "Maybe it's still good?" A qualitative study of factors influencing food waste and application of the E.P.A. Food Recovery Hierarchy in U.S. supermarkets. *Appetite, 161*, 105111. Doi:10.1016/j.appet.2021.105111

[15]. F.G. Areed, F., S. El-Kasassy, M., & A. Mahmoud, Kh. (2012). Design of neuro-fuzzy controller for a rotary dryer. *International Journal of Computer Applications, 37*(5), 34–41. Doi:10.5120/4606-6584

[16]. Adeodu, A. O. et al. (2019). Development and performance evaluation of Thermostat Controlled Rotary Dryer for agricultural produce. *Journal of Physics: Conference Series, 1378*(2), 022028. Doi:10.1088/1742-6596/1378/2/022028

[17]. Kiranoudis, C. T., Maroulis, Z. B., & Marinos-Kouris, D. (1996). Drying of solids: Selection of some continuous operation dryer types. *Computers & Chemical Engineering, 20.* Doi:10.1016/0098-1354(96)00040-3

[18]. Mirade, P. S., & Daudin, J. D. (2000). A numerical study of the airflow patterns in a sausage dryer. *Drying Technology, 18,* 81–97. Doi:10.1080/07373930008917694

[19]. Rindang, A., Panggabean, S., & Wulandari, F. (2019). CFD analysis of temperature drying chamber at Rotary Dryer with combined energy. *Journal of Physics: Conference Series, 1155,* 012037. Doi:10.1088/1742-6596/1155/1/012037

[20]. Cengel, Y. A., Ghajar, A.J. (2014). Chapter 4. In *Heat and Mass Transfer: Fundamentals & Applications, (5th ed.),* 237–260. McGraw-Hill Education.

[21]. Fedorko, G., Molnár, V., Kopas, M. (2018). Calculation and Simulation Model of a System RopeCon. *TEM Journal, 7*(3), 480-487. Doi:10.18421/tem73-02

[22]. Daneshjo, N., Malega, P., Hlubeňová, J., & Štuller, P. (2022). Implementation of simulation in the design of Robotic Production Systems. *TEM Journal, 11*(1), 179–188. Doi:10.18421/tem111-22

[23]. Malonjao, R. et al. (2022). Load cell mechatronic approach with Finite Element Analysis (FEA) in SolidWorks design development of a small-scale egg sorter. *International Journal on Recent and Innovation Trends in Computing and Communication, 10*(12), 115–124. Doi:10.17762/ijritcc.v10i12.5892

[24]. Mujumdar, A.S. (2006). Handbook of industrial drying, Boca Raton, Florida: CRC Press.